ROYAL SOCIETY
OF CHEMISTRY

PAPER

Check for updates

Double peak emission in lead halide perovskites by self-absorption†

Konstantin Schötz,[a] Abdelrahman M. Askar, [ID][b] Wei Peng,[c] Dominik Seeberger,[d] Tanaji P. Gujar,‡[d] Mukundan Thelakkat, [ID][d] Anna Köhler, [ID][ae] Sven Huettner,[d] Osman M. Bakr,[c] Karthik Shankar [ID][b] and Fabian Panzer [ID]*[a]

Despite the rapidly increasing efficiencies of perovskite solar cells, the optoelectronic properties of this material class are not completely understood. Especially when measured photoluminescence (PL) spectra consist of multiple peaks, their origin is still debated. In this work, we investigate in detail double peak PL spectra of halide perovskite thin films and single crystals with different material compositions. By different optical spectroscopic approaches and quantitative models, we demonstrate that the additional PL peak results from an extensive self-absorption effect, whose impact is intensified by strong internal reflections. This self-absorption accounts for the unusual temperature dependence of the additional PL peak and it implies that absorption until far into the perovskite's Urbach tail is important. The internal reflections entail that even for thin films self-absorption can have a significant contribution to the PL spectrum. Our results allow for a clear assignment of the PL peaks by differentiating between optical effects and electronic transitions, which is a necessary requirement for understanding the optoelectronic properties of halide perovskites.

1. Introduction

Halide perovskites, and optoelectronic devices based on them such as solar cells, LEDs, lasers or detectors, have undergone a tremendous development in the last few years. For this, their optical properties, in particular the absorption and photoluminescence (PL) spectra, play an important role when investigating the perovskite materials such as to derive conclusions about their electronic structure.[1,2] For example, phase transitions and different structural states can be identified by the associated optical spectra, which are experimentally easily accessible. Furthermore, from the analysis of the spectra, important material parameters can be determined, such as electron phonon coupling constants or dynamic and static disorder (in particular by temperature-dependent investigations).[3–8] PL signatures of different defect states both at higher and especially at lowest

temperatures were identified,[6,9,10] and the interaction of the perovskite with its environment (solvent, humidity or atmosphere) was investigated using PL measurements.[11–13] More recently, spatially resolved PL investigations allowed to associate the occurrence of defect assisted, non-radiative decay channels with the grain boundaries of the perovskite.[14] This has facilitated the development of appropriate passivation strategies, which in turn have led to the last significant increases in efficiencies of perovskite solar cells.[15–17]

However, although PL spectroscopy has been used intensively and versatilely in the past, it is still common for PL spectra measured under nominally identical conditions to differ from work to work or from group to group, and in many cases to exhibit several peaks within a PL band. Hence, there is still an intense discussion and disagreement about the origin of these multiple PL features, and a variety of interpretations exists. Some suggest the additional PL features to stem from the coexistence of a direct and an indirect bandgap,[18–22] defect induced recombination of (bound) excitons,[21,23–25] different electronic structure between the bulk and the surface,[26–28] coexistence of different crystalline phases[10,29] and to self-absorption effects.[30–33] Evidently, clarification on the origin of the multiple peak structure is urgently needed to allow for further understanding of the optoelectronic structure of lead halide perovskites.

In this work, we demonstrate that the occurrence of double peak structure is a general phenomenon in lead halide perovskites and not limited to single crystals or a specific material composition. We systematically address the different existing

[a] *Soft Matter Optoelectronics, University of Bayreuth, 95440 Bayreuth, Germany. E-mail: fabian.panzer@uni-bayreuth.de*

[b] *Department of Electrical and Computer Engineering, University of Alberta, Edmonton, AB T6G 1H9, Canada*

[c] *King Abdullah University of Science and Technology (KAUST), Division of Physical Sciences and Engineering, Thuwal 23955-6900, Kingdom of Saudi Arabia*

[d] *Department of Chemistry, University of Bayreuth, 95440 Bayreuth, Germany*

[e] *Bayreuth Institute of Macromolecular Research (BIMF) and Bavarian Polymer Institute (BPI), University of Bayreuth, 95440 Bayreuth, Germany*

† Electronic supplementary information (ESI) available. See DOI: 10.1039/c9tc06251c

‡ Current address: Shardabai Pawar Mahila College, Shardanagar, Baramati, Pune-413115 (MS), India.

interpretations and show that neither the recombination *via* different types of defects, or different electronic states between the bulk and the surface can account for the double peak structure. Instead, from temperature dependent one-photon-induced and two-photon-induced PL measurements, optical modelling, and a systematic change of measurement geometry, we conclude that the additional PL feature is due to a surprisingly extensive self-absorption effect, significantly amplified by internal reflections of PL. Finally, we show that by changing the refractive index of the perovskite environment, and thus the internal reflectivity, the relative intensity of the two peaks can be modified, further underpinning our approach.

2. Results and discussion

2.1 The double-peak structure

Fig. 1a shows the room temperature photoluminescence (PL) of four different lead halide perovskites used in this study, namely a $MAPbI_3$ thin film, a $MAPbI_3$ single crystal, a single crystal with a different halide, $MAPbBr_3$, and a single crystal with a different organic cation, $EA_{0.17}MA_{0.83}PbI_3$. For all samples, we observe the emission to be structured, *i.e.* to consist of a dominant higher energy peak that we will refer to as "Peak 1" and of a weaker lower energy peak or shoulder, henceforth called "Peak 2". This emission structure occurs independently of chemical composition and film structure for our four model samples, stressing the general nature of the phenomenon. The energy of

the emission band varies with sample composition. For the iodide perovskites, Peak 1 is located at 1.56 eV in the case of the single crystals, and at 1.58 eV for the thin film. While for the single crystals, Peak 2 appears as distinct peak at 1.48 eV, in the case of the thin film Peak 2 is located at 1.53 eV, *i.e.* less separated from corresponding Peak 1 and it is thus observed as a shoulder. For clarity, an alternative version of Fig. 1a with a logarithmic PL scale can be found in the ESI† (Fig. S1). For $MAPbBr_3$, Peak 1 and Peak 2 are located at 2.29 eV and 2.21 eV respectively. The relative PL intensity of Peak 2 compared to Peak 1 is in the range between 30 to 60% for all samples, depending on the position of excitation and detection spot and the angle of detection (see Fig. S2, ESI†).

To further investigate the two PL peaks, we performed temperature dependent PL measurements on all samples. Exemplarily, the results for the $MAPbI_3$ single crystal are shown in Fig. 1b (see Fig. S3 (ESI†) for the results of the other compounds). Upon cooling from 300 K to 160 K (Fig. 1b), where $MAPbI_3$ is in the tetragonal phase, the PL intensities of both peaks increase by an order of magnitude. Even without further analysis, it is evident that Peak 1 shifts to lower energies upon cooling, while the opposite is the case for Peak 2. Separating the spectra into the contributions of two individual peaks (see Fig. S4, ESI†) shows that Peak 1 shifts continuously to lower energies by 32 meV upon cooling, while Peak 2 shifts to higher energies by 10 meV until 240 K and then stays energetically constant (Fig. 1c).

Upon cooling below 160 K, $MAPbI_3$ undergoes a phase transition from a tetragonal to an orthorhombic crystal structure,[34]
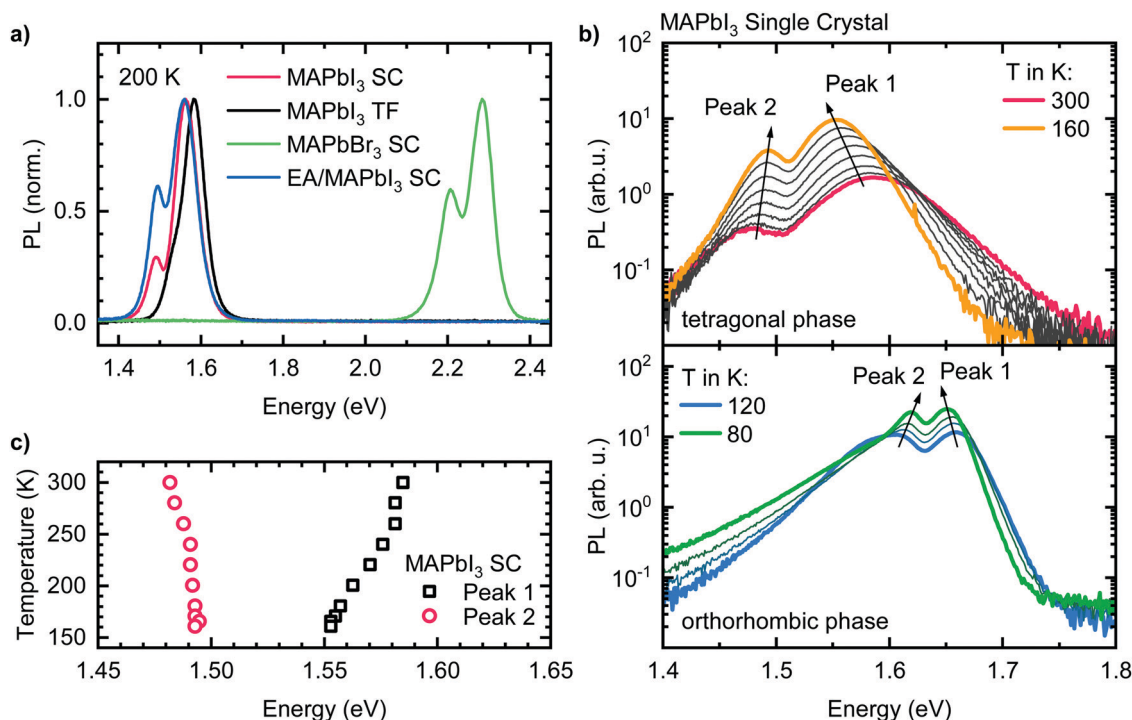

Fig. 1 (a) Normalized PL spectra of four different lead halide perovskite samples showing double peak emission. (b) Temperature-dependent PL of a $MAPbI_3$ single crystal between 300 K (red) and 160 K (orange), *i.e.* tetragonal phase in steps of 20 K (top) and in the orthorhombic phase between 120 K (blue) and 80 K (green). (c) Temperature-dependent peak position of Peak 1 and Peak 2 from the PL shown in (b) after spectral decomposition.

2290 | *J. Mater. Chem. C*, 2020, **8**, 2289–2300

This journal is © The Royal Society of Chemistry 2020

which is accompanied by an 100 meV increase of the band gap, directly impacting on the absorption and PL properties.[35–37] Until 120 K a transition region exists in which the different phases coexist leading to PL spectra with more than two PL features (Fig. S5, ESI†). Between 120 K and 80 K we again observe two PL-Peaks, which exhibit the same spectral temperature dependence as Peak 1 and Peak 2 in the tetragonal phase (*i.e.* shift to lower (higher) energies of Peak 1 (Peak 2) with decreasing temperature). Below 80 K additional PL features appear, leading to relatively complex PL spectra at lowest temperatures (Fig. S6, ESI†). It becomes obvious that additional well-resolved/distinct PL bands can be observed over the entire investigated temperature range, *i.e.* also over different crystal phases.

2.2 Investigating possible structural origins for the double peak

Several interpretations have been proposed to account for the structure in the emission bands. We shall evaluate whether these interpretations are consistent with our data one by one.

2.2.1 Coexistence of radiative direct and indirect transitions.
Several works associated additional PL bands with the coexistence of a direct and an indirect band gap in halide perovskites.[19,20] Indeed, Rashba splitting in halide perovskites, from which an indirect band gap character follows, has been shown.[38–41] However, its extent and impact on the excited state properties of the perovskites is debated[18,40–48] and some more recent publications suggest an insignificant impact of the Rashba splitting on the optical properties of the perovskite.[42,49] Theoretical works suggested that an impact of the Rashba splitting on the perovskite PL disappears at higher excitation densities, namely around 10^{18} cm^{-3}.[50] The PL spectra in Fig. 1 were measured with an excitation density of $n = 4.8 \times 10^{18}$ cm^{-3} (see ESI† for details), so that we do not expect the Rashba splitting to play a significant role in the PL. Furthermore, Peak 2 is clearly present even at higher excitation densities (*vide infra*), which indicates that Rashba splitting does not cause the appearance of Peak 2. Moreover, the coexistence of a radiative direct and indirect transition would imply a competition between both pathways, as it is *e.g.* reported for Ge$_{1-x}$Sn$_x$ alloys.[51,52] Regarding the temperature dependence, cooling should favor electron trapping in the energetically lower indirect bandgap valley, resulting in a decreased relative contribution of the higher energy direct bandgap transitions. Concomitantly, the PL intensity should drop for an indirect character of the PL, as the phonon-assisted radiative recombination is less efficient at lower temperatures.[51–54] This is at variance with the experimental observation shown in Fig. 1. Thus, we can exclude the double peak emission to be associated with the coexistence of an indirect and direct band gap.

2.2.2 Strain-induced defects in the bulk.
Recently, the significance of strain-induced defects and their impact on the excited state recombination properties of halide perovskites were reported.[55,56] To probe whether recombination at strain-induced defects may be at the origin of the double-peak structure, we measured the PL of perovskite thin films that were deposited either on glass, or on polyethylene terephthalate

(PET). These substrate materials exhibit different thermal expansion coefficients in the order of 10^{-5} K^{-1} (PET),[57,58] and 10^{-6} K^{-1} (glass),[59] respectively. With the thermal expansion coefficient of MAPbI$_3$ being in the range of $(1.6 \times 10^{-4}$–$3.8 \times 10^{-4})$ K^{-1},[60,61] we expect a larger build-up of strain upon cooling for the MAPbI$_3$/glass sample compared to the MAPbI$_3$/PET sample.[62] The degree of strain in a sample can be correlated to the temperature at which the tetragonal to orthorhombic phase transition occurs upon cooling.[3,63] We identify the critical temperature T_c and the width of the tetragonal to orthorhombic phase transition from temperature dependent absorption measurements following the same approach as in previous works (also see Fig. S7, ESI†).[3,64] We find a lower T_c and an increased width of the transition for the MAPbI$_3$/glass sample ($T_{c,Glass}$ = 145.9 $\pm$ 0.3 K, FWHM$_{Glass}$ = 10.1 $\pm$ 0.7 K) compared to MAPbI$_3$/PET ($T_{c,PET}$ = 147.2 $\pm$ 0.2 K FWHM$_{PET}$ = 8.8 $\pm$ 0.6 K). Furthermore, we analyzed the temperature dependence of the PL peak positions of the two samples, where we find a shift of 0.25 meV K^{-1} for the sample on the glass substrate and a shift of 0.28 meV K^{-1} for the sample on the PET substrate. Both, the decrease in T_c and the reduced temperature dependence of the PL peak position in the MAPbI$_3$/glass sample imply that there is indeed more strain in the MAPbI$_3$/glass sample. Fig. 2a shows the normalized PL spectra of the MAPbI$_3$/glass and MAPbI$_3$/PET samples at 170 K. This is the temperature where we expect the highest strain to have built up upon cooling, without already inducing the tetragonal–orthorhombic phase transition. For both thin film samples, Peak 2 appears as shoulder, similar to the thin film sample in Fig. 1. A decomposition of the spectrum into two peaks shows that Peak 2 is about 10–15% more intense in the MAPbI$_3$/glass sample (see Fig. S8, ESI†). Upon cooling, the intensity of Peak 2 relative to Peak 1 increases continuously and, importantly, in the same manner for both samples (Fig. 2b). If Peak 2 was related to strain-induced defects, it should evolve differently with temperature in the sample with the larger strain. This is at variance with the observation of an identical temperature-evolution for both samples, and thus implies that strain-induced defects are not the cause for the double-peak structure.

2.2.3 Surface defect states.
To address whether surface defect states, and the associated recombination *via* bound excitons, may be responsible for the occurrence of Peak 2, we passivated the surface of MAPbI$_3$ single crystals. We used either a cyclohexane solution of the electron-accepting benzothiadiazole or the electron-donating, liquid mono-thiophene to selectively passivate negatively and positively charged surface defects, respectively.[16,65] We measured the PL directly before and after dropping the respective liquids onto the single crystals (Fig. 2c and d), ensuring that the crystals, the laser and the detector did not move during this process. When dropping benzothiadiazole onto the single crystals, both, Peak 1 and Peak 2 remain nearly unchanged in their energy and intensity (Fig. 2c). This suggests that negatively charged surface defects are either not present or do not affect the spectral shape of the PL. In the case of thiophene, the energetic position and the intensity of Peak 2 hardly changes. However, the intensity of Peak 1 more
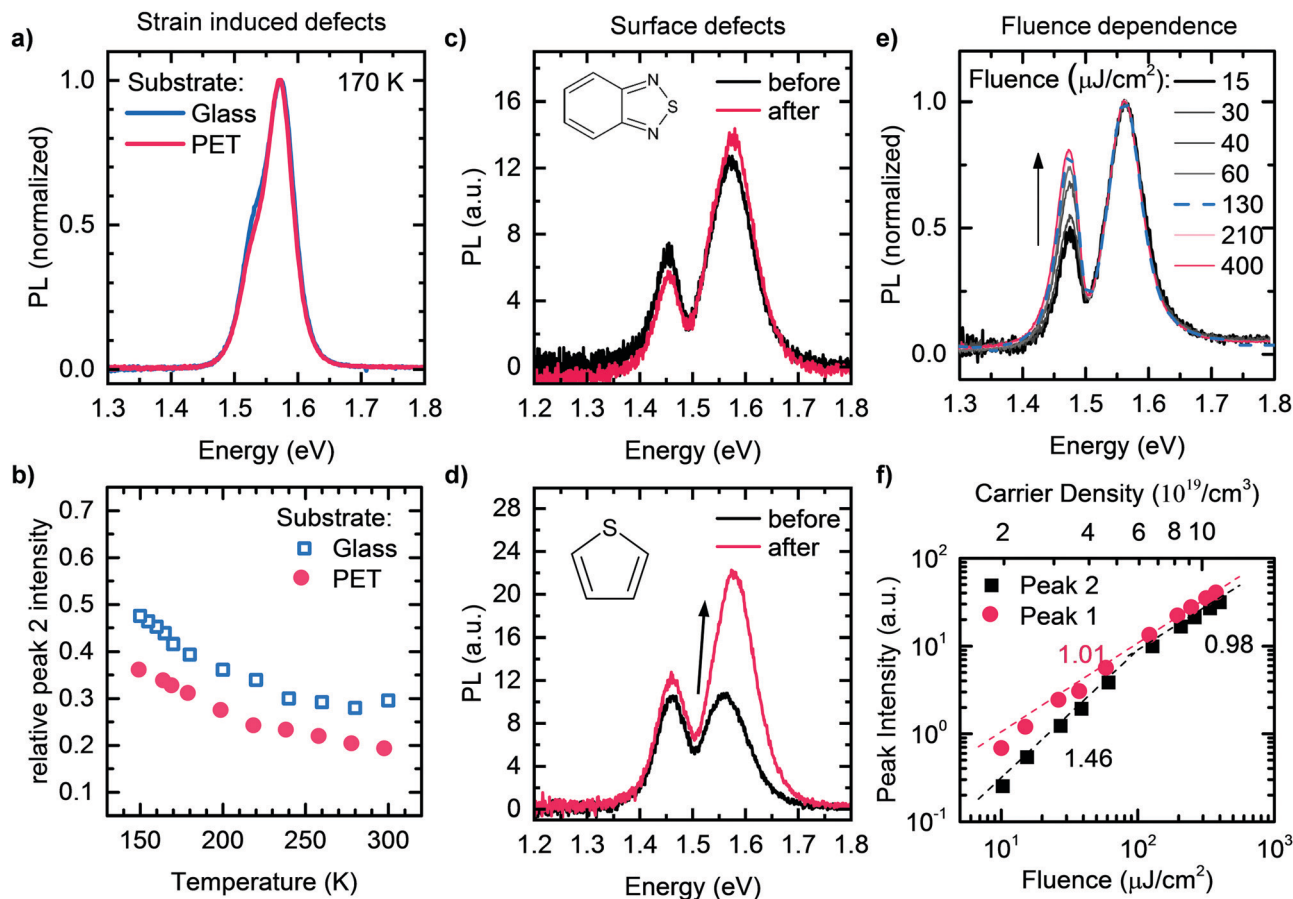
Fig. 2 (a) PL of MAPbI$_3$ thin films at 170 K processed on glass (blue) and on PET (red). (b) Temperature dependence of the PL Peak 2 intensity relative to Peak 1 intensity of the two thin films processed on glass (blue squares) and PET (red dots). (c and d) Room temperature PL of a MAPbI$_3$ single crystal before (black) and after (red) surface passivation with (c) benzothiadiazole dissolved in cyclohexane and (d) mono-thiophene. (e) Fluence dependent PL (normalized) of a MAPbI$_3$ single crystal at 200 K and (f) corresponding peak intensities as a function of laser fluence, plotted on a double logarithmic scale. The dashed lines represent fits with slope values as indicated.

than doubles, and the peak position shifts by about 15 meV to higher energies (Fig. 2d), as expected for a successful surface passivation (see Fig. S9 (ESI†) for a discussion on the observed blue shift of Peak 1). Evidently, emission from Peak 1 is affected by positively charged defects on the surface of the MAPbI$_3$ single crystals, most likely due to iodine vacancies as proposed in the past,[16] while emission from Peak 2 is hardly affected. From this passivation experiment, we can deduce that the higher-energy Peak 1 is associated with emission near the crystal surface, while the lower-energy Peak 2 may be associated with emission that is predominantly from the bulk of the crystal. However, it is not clear, whether only the spatial origin of the emission differs for the two peaks, or whether they also result from actual different electronic states, as has been suggested in the past.[28,66]

2.2.4 Surface *versus* bulk emission. To follow up the question whether the two peaks may originate from emission near the surface and in the bulk, we performed temperature dependent two-photon-induced photoluminescence (2PI-PL) measurements and compared them with the results from one-photon-induced photoluminescence (1PI-PL) experiments. In the more common 1PI-PL experiments, a sample volume near the surface is excited, determined by the exponential fall-off in

the absorbed light well known as Lambert–Beer's law. In contrast, for a 2PI-PL experiment, a high excitation intensity is required, which is typically achieved by focusing of a laser beam. Thus, only a small, well-defined spot in the sample bulk is excited.[67] Even though the two processes follow different selection rules and thus excite different transitions, in either case, electrons and holes are generated that thermalize in the band and subsequently recombine *via* the same radiative transition.[68,69] The results of the temperature dependent 2PI-PL-experiment are shown exemplarily for the tetragonal phase at 200 K and for the orthorhombic phase at 80 K together with the corresponding scaled 1PI-PL spectra in Fig. 3a and b respectively. The peak position of the 2PI-PL resembles very well Peak 2 from the 1PI-PL at both temperatures (*i.e.* both crystal phases). This demonstrates that Peak 2 is associated with the bulk. However, from these results it is still not distinguishable whether Peak 2 results from different distinct transitions occurring at the bulk and the surface, or to which extend self-absorption effects modulate the PL spectra, contributing to the observation of Peak 2.

2.2.5 Strain-independent defects in the bulk. To address, whether Peak 2 may be caused by recombination at defects in

2292 | *J. Mater. Chem. C*, 2020, **8**, 2289–2300

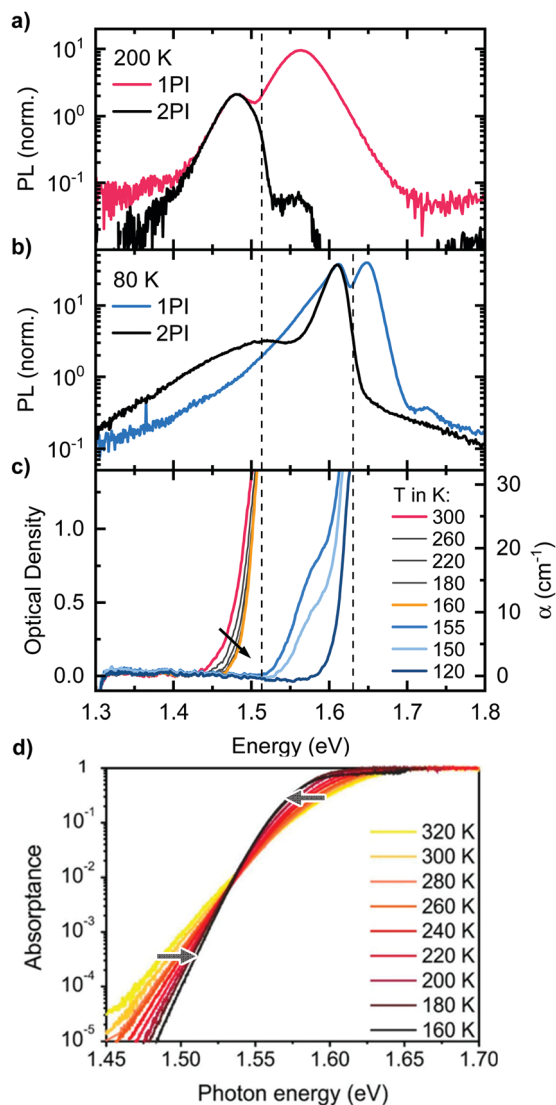This journal is © The Royal Society of Chemistry 2020

Fig. 3 One-photon-induced (1PI) and two-photon-induced (2PI) PL of a MAPbI$_3$ single crystal, (a) at 200 K (tetragonal phase) and (b) at 80 K (orthorhombic phase). (c) Optical density of a MAPbI$_3$ single crystal in the temperature range from 300 K to 120 K. The arrow indicates reducing temperature. (d) Temperature-dependence of the Urbach-tail absorption. Reprinted with permission from Ledinsky et al.,[74] Copyright 2019 American Chemical Society.

the bulk that are independent of any mechanical strain, we recorded the PL at 200 K as a function of laser fluence (Fig. 2e) and analyzed the corresponding PL intensities of Peak 1 and Peak 2. This is shown in Fig. 2f on a double logarithmic scale. For laser fluences up to 120 μJ cm^{-2}, Peak 2 grows with a slope of 1.46, while the intensity of Peak 1 increases with a slope of 1.01. For higher fluences, both peaks grow with a slope of about 1. Usually, when an emission feature results from recombination at defect sites, its relative contribution to the overall PL decreases with increasing laser fluence as such traps are filled up.[6,10] This would result in a sublinear slope for the defect-based emission, at variance with our experiment, where we observe a superlinear slope. This speaks against assigning the origin of Peak 2 to recombination at defects in the bulk.

2.3 Addressing optical effects as possible origin for the double-peak structure

So far, we could establish that Peak 2 results from the bulk while Peak 1 is associated with PL near the surface. We did not find any structural causes in the bulk that could account for Peak 2. We therefore consider whether self-absorption may be associated with the occurrence of the double peak structure. For this, it is obviously useful to consider the absorption of the perovskite crystals. Thus, we determined the temperature-dependent optical density of the MAPbI$_3$ single crystal by transmission measurements (Fig. 3c). With our experimental setup, we can reliably determine optical densities (OD) in the range from about 0.1 to 1.5. This corresponds to absorption coefficients α in the range of 1 to 30 cm^{-1}, considering a thickness of 1 mm, which is typical for the single crystals we used. Such low α-values occur in the Urbach tail of MAPbI$_3$, which has been characterized in the past using photothermal deflection spectroscopy (PDS) or external quantum efficiency (EQE) measurements.[70–72] At 300 K, detectable absorption for our setup starts at 1.44 eV and rises steeply to an OD of 1.5 at 1.5 eV. Importantly, upon cooling, the detectable absorption shifts to higher energies and the absorption edge becomes steeper. Below 160 K, the absorption jumps to 1.63 eV, indicating the transition to the orthorhombic phase.[34,35] This is accompanied by an additional well-resolved shoulder at 1.58 eV that matches the energy for absorption of the tetragonal phase of thin films at this temperature.[4,73] Evidently, some small residues of tetragonal phase still prevail at 155 K and 150 K. An estimation considering a crystal thickness of 1 mm and the absorption coefficient of MAPbI$_3$ as reported by Crothers et al.[70] implies that approximately 0.1% of tetragonal phase are still present at 155 K. The shift of the measured absorption of the single crystal to higher energies upon cooling from 300 K to 160 K is opposite to the trend observed for the absorption edge of thin films. However, it can be understood when considering which part of the absorption spectrum we probe with our transmission measurement: both the estimated values of the absorption coefficient and the energetic position of the absorption edge indicate that we measure Urbach tail absorption below the so called Urbach focus point, which was found for MAPbI$_3$ to be around 1.54 eV, where the absorption coefficient takes a value of α = 500 cm^{-1}.[60,74] For absorption coefficients below this point, the temperature-dependence of the absorption is inversed, i.e. the absorption edge shifts to higher energies upon cooling, in accordance with our results. For clarification, the temperature-dependence of the Urbach-tail, including the Urbach focus point, is displayed in Fig. 3d, taken from Ledinsky et al.[74] The arrows indicate the temperature-evolution above and below the Urbach focus point. We also would like to emphasize that the measured absorption edge of the single crystal only represents a small part of the Urbach tail and cannot be used to determine the optical band gap of the material and thus does not imply a red shifted band gap of the single crystal compared to thin films.

The temperature dependent absorption spectra reveal two important facts: first, significant absorption, which reduces the transmission of photons generated deep in the crystal bulk to less

This journal is © The Royal Society of Chemistry 2020

J. Mater. Chem. C, 2020, 8, 2289–2300 | 2293

Paper

than 10%, occurs in the same energetic range as the high energy edge of the 2PI-PL, both for the tetragonal (1.51 eV) and the orthorhombic phase (1.63 eV) as indicated by dashed lines in Fig. 3. This is essentially the position of the minimum between Peak 1 and 2. A similar observation was reported for MAPbBr$_3$ single crystals by Yamada *et al.* comparing transmission with 2PI-PL measurements.[33] Second, the shift of the absorption to higher energies upon cooling from 300 K to 160 K, matches well with the temperature dependence of the energetic position of Peak 2 in Fig. 1c. These two observations are a strong indication that the occurrence of Peak 2 is correlated to a self-absorption effect.

To test the plausibility of self-absorption as origin of Peak 2, we modelled our 1PI-PL by explicitly considering the effect that self-absorption will have on emission generated throughout the crystal as illustrated in Fig. 4. To do so, we calculated the one-dimensional charge carrier distribution $n(x)$ that results from laser excitation. For this, we considered the absorption coefficient of MAPbI$_3$ at 337 nm, which can be found *e.g.* in Crothers *et al.*,[70] and the Beer–Lambert-law. This charge carrier distribution leads to photoluminescence *via* bimolecular recombination. The PL generated by recombination at a site x' can then travel towards either to front or the backside of the crystal, which are taken to be 1 mm apart. This is about the size of the single crystals examined in this study. On the way through the crystal, the perovskite absorbs part of the PL, thus attenuating it. At the interface between perovskite and surrounding media, the PL is either transmitted or reflected with a certain probability. A key feature of our model is that we allow for multiple inner reflections. The PL that is detected at the front surface is then a superposition of the PL that leaves the crystal at the front without internal reflections, PL$_{direct}(E)$, and the PL that leaves the crystal after (multiple) internal reflections, PL$_{filtered}(E)$.

$$\text{PL}_{detected}(E) = C \cdot \text{PL}_{direct}(E) + \text{PL}_{filtered}(E). \tag{1}$$
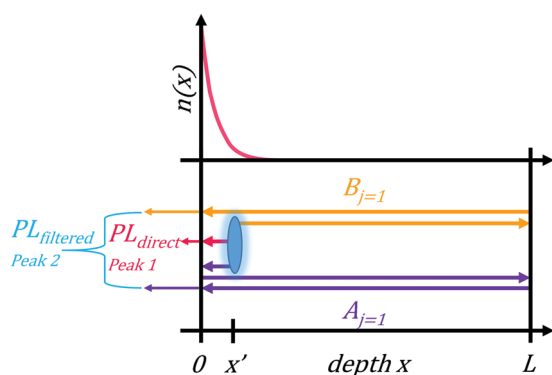

Fig. 4 Illustration of the optical paths considered in the optical modeling. From a certain depth in the crystal x', the PL can either hit the front surface and escape with a certain probability (red), contributing to Peak 1 (PL$_{direct}$), or can be reflected and travel towards the back surface. There it is reflected with a certain probability and travels back to the front surface, where it is either transmitted (purple) and contributes to Peak 2 (PL$_{filtered}$), or reflected again. Alternatively, the PL originating from x' can travel to the back, being reflected and traveling to the front, where it likewise can either escape (orange), contributing to Peak 2, or be reflected. On its way through the crystal, the PL is filtered by the absorption of the perovskite.

The constant C was found necessary to allow for a mismatch between excitation spot and detection spot. PL$_{direct}(E)$ and PL$_{filtered}(E)$ are calculated according to the Beer–Lambert law,

$$\text{PL}_{direct}(E) = \int_0^L \text{PL}_{int}(E) \cdot n(x)^2 \cdot (1 - r_f) \cdot \exp[-\alpha(E) \cdot x]\mathrm{d}x \tag{2}$$

$$\text{PL}_{filtered}(E) = \int_0^L \sum_{j=1} \text{PL}_{int}(E) \cdot n(x)^2 \cdot (1 - r_f) \cdot \{A_j + B_j\}\mathrm{d}x, \tag{3}$$

where $A_j = r_f^j \cdot r_b^j \cdot \exp[-\alpha(E) \cdot (2jL + x)]$ considers the part of the PL that propagates from the site of generation, x', towards the front surface. Propagation towards the back surface is considered by $B_j = r_f^{j-1} \cdot r_b^j \cdot \exp[-\alpha(E) \cdot ((2j - 1)L + (L - x))]$. Here, $\alpha(E)$ denotes the absorption coefficient of the material, r_f and r_b are the reflection probabilities at the front and back interface, respectively, and L denotes the length of the crystal. j denotes the number of reflections at the back interface. For the intrinsic PL lineshape PL$_{int}(E)$, we assume a hyperbolic secant fitted to Peak 1, see Fig. S4 (ESI†). Even though there is no immediate physical meaning to this lineshape, this phenomenological approach reproduced the spectral shape better than a Gaussian, Lorentzian or Voigt lineshape function. For the absorption spectrum $\alpha(E)$, we took the spectrum, especially of the Urbach tail, reported by Ledinsky *et al.*[74] and normalized it to the absolute values from Crothers *et al.*,[70] which are not available in the region of Urbach absorption. The average reflection probabilities r_f and r_b were calculated *via* the Fresnel equations with a refractive index of 2.5 for MAPbI$_3$ in the relevant energy range,[75] and of 1 for air. Averaging over all angles of incidence, we obtain a reflection probability of 0.85 for the perovskite–air interface. This high reflection probability demonstrates the importance of considering multiple inner reflections, where up to $j_{max} = 10$, an increase of Peak 2 can be observed. However, for our calculation, we considered $j = 20$ reflections to be well above j_{max}. We note that this approximation does not consider that PL reaching the interface with a larger angle also travelled a larger distance through the material. However a slightly bigger (smaller) reflection probability can be easily compensated by a slightly smaller (bigger) crystal to obtain a similar result. For comparison with experimental PL spectra, the calculated spectrum PL$_{detected}(E)$ is finally normalized to the experimental data. We note that for infinitely large, perfect and parallel front and back surfaces, photons that hit the surface outside the escape cone would not be able to leave the sample. In reality however, when hitting irregularities, such as grain boundaries in the case of thin films, or when reaching the edges or side surfaces of single crystals, the photons can escape the perovskite even after multiple inner reflections.

The comparison between the PL spectrum calculated using our model (with a value of $C = 0.66$) and the experimental PL spectrum of the MAPbI$_3$ single crystal at room temperature is shown by the black squares and the black line in Fig. 5a. The excellent agreement for this simple model – which only uses a

2294 | *J. Mater. Chem. C*, 2020, **8**, 2289–2300

This journal is © The Royal Society of Chemistry 2020

single "fitting" factor in the form of C – clearly demonstrates the significant importance of self-absorption. Fig. 5b indicates which part of the PL results from the directly transmitted PL, $PL_{direct}(E)$, and from PL that suffered internal reflections and self-absorption, $PL_{filtered}(E)$. We stress again here the key role of considering multiple reflections. Effects that are neglected in our model are carrier diffusion, photon recycling and internal scattering. Carrier diffusion and photon recycling both have similar effects insofar that they can generate PL at a site that is different from the original absorption. While photon recycling can have significant impact on the PL properties[76,77] and should, together with carrier diffusion, enhance the intensity of Peak 2, we found it was not necessary to include photon recycling explicitly to model our measured spectra.

To further test whether self-absorption, magnified by reflection at the crystal back surface, is indeed causing the double peak structure, we repeated the room temperature 1PI-PL of the same MAPbI$_3$ single crystal while modifying the outcoupling, and thus the reflection, at the back surface. For this, we placed a drop of glycerin at the backside of the crystal, while we excited the sample and detected resulting PL at the front side, identical to the previous measurement. This measurement was performed directly after the one without glycerin drop without moving the crystal or detection, to exclude any influence of a changed measurement geometry. The refractive index of glycerin is 1.47,[78] *i.e.* higher than the one of air, which reduces the reflection probability at the backside of the crystal from 0.85 to 0.70. According to our model, this should lead to a decreased intensity of Peak 2, accompanied by a spectral shift to higher energies. The obtained experimental data and the model data (keeping all parameters identical to before, except of the reflection probability), are shown as red line and dots in Fig. 5a. We find the intensity of Peak 2 to reduce to half the previous value and to shift to the blue by 10 meV. This observation is excellently captured by our model.

These findings represent compelling evidence that Peak 2 originates from an extreme self-absorption effect, which is caused by significant internal reflections in the temperature ranges investigated in this study. We stress that below about 80 K, the temperature-dependence of Peak 2 changes, probably due to an increasing contribution of PL of bound exciton states,[79] which becomes increasingly efficient at lower temperatures. In passing we mention that changes in reflectivity for example due to the addition of thiophene or benzothiadiazole, or due to different substrates such as Glass and PET can easily account for the slightly different intensities of Peak 2 that we observed in Fig. 2a and b.

With the insight provided by our results on the different origin of Peak 1 and 2, we can understand the different temperature dependence of Peak 1 and 2 in their PL spectra, with Peak 1 shifting to the red spectral range and Peak 2 to the blue upon cooling. Peak 1, resulting from $PL_{direct}(E)$, is modified by reabsorption only from the point where it was created, to the front surface. Reabsorption thus occurs over a typical lengthscale of about 50 nm, depending on the wavelength of excitation. A significant attenuation, say, to a level of 10% of transmitted intensity, would be then obtained for absorption coefficients above about of 5×10^5 cm^{-1}. If diffusion of charge carriers is considered, the lengthscale increases to the µm range, and the relevant absorption coefficient decreases to about 10^4 cm^{-1}. In contrast, reabsorption for Peak 2 occurs over a length scale exceeding the crystal thickness of 1 mm, thus becoming relevant for absorption coefficients as low as a few 10 cm^{-1}. Fig. 3d, taken from Ledinsky *et al.*, shows the evolution of the Urbach tail with temperature.[74] The two arrows indicate the typical absorption coefficients associated with self-absorption for $PL_{direct}(E)$, which causes Peak 1, and for $PL_{filtered}(E)$ that gives rise to Peak 2. One can see that the two ranges for the absorption are on different sides of the Urbach focus point. As a result, cooling causes a blue-shift for Peak 2 due to filter effects, despite Peak 1 shifting to the red due to the decreasing bandgap of the perovskite.

In the framework of filtered PL which we present here, also the dependence of the relative intensity of Peak 2 from the
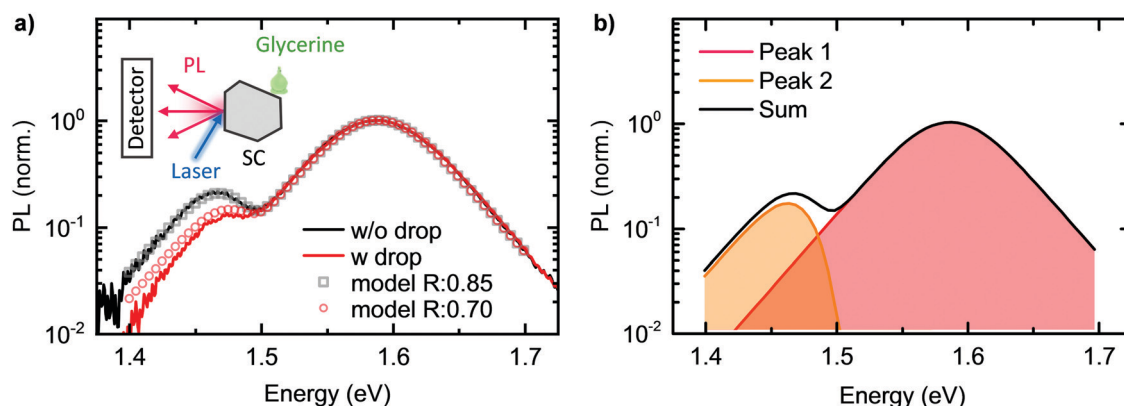

Fig. 5 (a) PL spectrum of a MAPbI$_3$ single crystal in air at room temperature (black solid line) together with the modelled PL with an internal reflection probability of 0.85 (black open squares). The PL spectrum of the same crystal with a drop of glycerin at the back is displayed as red solid line, together with the modeled PL with an internal reflection probability at the back interface of 0.7 (red open circles). (b) Decomposition of the modelled PL into the contribution of the PL coming directly from the excitation spot (PL_{direct}, Peak 1, red) and the PL after internal reflections and self-absorption ($PL_{filtered}$, Peak 2, orange).

excitation spot and/or the detection angle can be understood easily. Due to the high refractive index of the perovskite, the direct PL is limited to its escape cone at the spot where the PL is generated. In contrast, the filtered PL can travel large distances and thus can also leave the crystal far away from the excitation spot or at the side surfaces of the crystal. This is in agreement with a very recent study by Kojima *et al.*, where the authors demonstrate by angle dependent PL of a MAPbBr$_3$ crystal, that direct PL is limited to a small escape cone, whereas filtered PL is also detected from the side and the backside of the crystal.[80]

If we apply our model to fit the PL of the MAPbI$_3$ thin film from Fig. 1a, it turns out that we need to set the sample thickness to 3.5 μm to model the experimental data satisfyingly. However, the actual thickness of the sample is 0.7 μm, indicating that our model is over-simplified for the application for thin films. This points towards the importance to also consider the lateral component of the propagation direction of the light.

We finally note that the long optical pathways in halide perovskites can also impact their photocurrent measurements. For excitation in the spectral range of the Urbach tail, penetration lengths can be on the length scale of mm, so that the entire sample volume is excited and contributes to charge carrier generation. This can overcompensate the higher density of generated charges for excitation at higher photon energies, where the absorption coefficient is bigger, but the penetration length is limited to tens of nanometers. A peak of the photocurrent in the spectral region of the Urbach tail would be the consequence, bearing danger of misinterpretation if optical effects are not considered.

3. Conclusion

In summary, we have shown that the often observed double peak PL spectra of halide perovskites result from a significant self-absorption effect, which is amplified by the high internal reflection probability of PL in the sample, with Peak 1 being the emission directly outcoupled, and Peak 2 being emission that suffered multiple internal reflections and pronounced self-absorption. This effect not only impacts on the spectra of single crystals but also occurs in thin film spectra, and it is not limited to a specific perovskite composition, thus rendering it a general phenomenon. We found absorption from the Urbach-tail of the perovskite to be highly relevant for the self-absorption-effect, because optical paths in the sample can easily be on the length scale of millimeters. By controlled reduction of the reflection probability at the back side of a single crystal we could experimentally alter the intensity of the additional PL peak, thus providing compelling evidence for our conclusion. Using a relatively simple quantitative model, we were also able to simulate the PL spectra including the additional peaks and the spectral shifts that were observed in the experiment upon changing the reflectivity. Our results will help to interpret photoluminescence spectra of lead halide perovskites correctly by delivering a better understanding of the effects and importance of self-absorption and internal reflections in this material class.

4. Experimental section

4.1 Sample preparation

MAPbI$_3$ single crystals were prepared following the inverse temperature crystallization technique.[81] In brief, the synthesis started with a 1–1.3 M solution of MAI (from Dyesol-Limited, Now GreatCell Solar) and PbI$_2$ (Sigma-Aldrich) in gamma-butyrolactone (GBL, Sigma-Aldrich). The precursors dissolved in GBL after 30 minutes of vigorous stirring at 60 °C. Upon filtering the solution using 0.22 μm PVDF filters, the stock solution was then distributed into small vials with 3–4 ml of solution each. The vials were kept undisturbed in an oil bath for 3–4 hours at 110 °C. Once the desired size of the crystals was achieved, the crystals were removed from the synthesis solution, washed quickly with fresh GBL, dried with a N$_2$ flow.

EA$_{0.17}$MA$_{0.83}$PbI$_3$ single crystals were grown using the antisolvent-vapor diffusion assisted crystallization method, as reported elsewhere.[82,83] In brief, the precursor solutions were prepared by dissolving proper amount of methylammonium iodide, ethylammonium iodide and PbI$_2$ in γ-butyrolactone in a ratio of 0.15 M : 0.15 M : 0.1 M. The precursor solutions were then loaded in a small crystallizing dish with aluminum foil cover, which was then placed in a bigger dish with antisolvent, namely dichloromethane, loaded. The whole setup was sealed with an aluminum foil cover. The inner cover was left with a ∼0.5 mm hole to let the antisolvent vapor diffuse inside the precursor solution. The growth process usually takes 4–6 days.

For the Synthesis of the MAPbBr$_3$ single crystals, a 1 M solution of MAPbBr$_3$ in DMF was prepared by mixing equimolar amounts of MABr and PbBr$_2$ in DMF over a period of 1 h. 5–10 ml of the solution were filtered over a 200 nm PTFE filter and placed in a glass Petri dish. The Petri dish was placed on a hotplate and set to 47.5 °C. The heat was increased slowly until the first nuclei were forming outside the mould. Then the temperature was increased to 75 °C with a rate of 5 °C per hour. The crystals were removed from the hot solution and washed with ether.

For fabrication of the MAPbI$_3$ thin films, the substrates were cleaned with detergent followed by sonication in deionized water, acetone and ethanol for 10 min each, and dried with clean dry air. After ozone treatment (at 50° for 15 min with 2 l per min O$_3$ flow), the substrates were transferred in a glovebox under N$_2$ atmosphere. For MAPbI$_3$ formation, we adapted a published procedure[84,85] and optimized it as follows. PbI$_2$ (1 M) was dissolved in *N,N*-dimethyl formamide overnight under stirring conditions at 100 °C and 80 μl solution was spin coated on the quartz substrates at 2000 rpm for 50 s, and dried at 100 °C for 5 min. 100 mg MAI powder (see ESI† for details) was spread out around the PbI$_2$ coated substrates with a Petri dish covering on the top and heated at 165 °C for 13 h for full conversion.

4.2 Photoluminescence and absorption measurements

The temperature-dependent 1PI-PL of all samples and the fluence-dependent PL were performed using a home-build setup. The samples were put in a continuous flow cryostat (Oxford Instruments, Optistat CF) connected to a temperature

controller (Oxford Instruments ITC503S). The sample is excited with a 337 nm nitrogen laser (LTB MNL 100). The signal is collected *via* a charge-coupled device (CCD) camera (Andor iDus DU420a-OE) coupled to a spectrograph (Andor Shamrock SR303i).

The passivation experiments and the experiments with the glycerin drop at the back of the crystal were performed on air at room temperature. The crystals were excited using the nitrogen laser (LTB MNL 100) and the emitted PL was collected with an optical fiber and detected by a CCD camera (Andor iDus DU420A-OE) coupled to a spectrograph (LOT Oriel MS125). For both measurements, the sample was not moved between initial and final measurement. For the passivation measurement, it was ensured that all liquid evaporated before the final PL measurement by waiting for five minutes.

For temperature-dependent 2PI-PL measurements, the perovskite crystals used for this experiment were placed in a continuous flow cryostat, connected to a temperature controller (Oxford Instruments MercuryITC). For excitation, we used a mode-locked titanium-sapphire laser (Coherent Chameleon Ultra), with its emission center wavelength adjusted to 1000 nm. The laser power was reduced to 26 mW at 4.73 MHz and focused to a spot with a beam waist of 0.01 mm at the position of the sample. For the transmission measurements of the single crystal, a broadly fluorescent material was placed in the cryostat and its PL was measured once without and once with crystal in front of it. This technique has the advantage against conventional transmission measurements that diffraction effects that deflect the transmitted light from the optical axis play only a little role.

For each set of experiments, a new crystal was used to exclude any influence of degradation effects by previous measurements on the results of the experiment. All PL data were corrected by the corresponding setup efficiency.

Author contributions

FP initiated, and planned the project. KoS performed all optical characterizations and derived the optical model. FP, AK and KoS discussed the project. AMA synthesized the MAPbI$_3$ single crystals under supervision of KaS. WP synthesized the EAMAPbI$_3$ single crystals under supervision of OMB. DS synthesized the MAPbBr$_3$ single crystals under supervision of SH. TG produced the MAPbI$_3$ thin films under the supervision of MT. FP and KoS wrote the manuscript which was revised by all authors. FP supervised the project.

Conflicts of interest

There are no conflicts to declare.

Acknowledgements

References

1 L. M. Herz, Charge-Carrier Dynamics in Organic–Inorganic Metal Halide Perovskites, *Annu. Rev. Phys. Chem.*, 2016, **67**, 65–89.

2 Y. Kanemitsu, Luminescence Spectroscopy of Lead-Halide Perovskites: Materials Properties and Application as Photovoltaic Devices, *J. Mater. Chem. C*, 2017, **5**(14), 3427–3437.

3 T. Meier, T. P. Gujar, A. Schönleber, S. Olthof, K. Meerholz, S. van Smaalen, F. Panzer, M. Thelakkat and A. Köhler, Impact of Excess PbI$_2$ on the Structure and the Temperature Dependent Optical Properties of Methylammonium Lead Iodide Perovskites, *J. Mater. Chem. C*, 2018, **6**(28), 7512–7519.

4 F. Panzer, C. Li, T. Meier, A. Köhler and S. Huettner, Impact of Structural Dynamics on the Optical Properties of Methylammonium Lead Iodide Perovskites, *Adv. Energy Mater.*, 2017, **7**(16), 1700286.

5 A. D. Wright, C. Verdi, R. L. Milot, G. E. Eperon, M. A. Perez-Osorio, H. J. Snaith, F. Giustino, M. B. Johnston and L. M. Herz, Electron-Phonon Coupling in Hybrid Lead Halide Perovskites, *Nat. Commun.*, 2016, **7**, 11755.

6 R. L. Milot, G. E. Eperon, H. J. Snaith, M. B. Johnston and L. M. Herz, Temperature-Dependent Charge-Carrier Dynamics in CH$_3$NH$_3$PbI$_3$ Perovskite Thin Films, *Adv. Funct. Mater.*, 2015, **25**(39), 6218–6227.

7 C. Wehrenfennig, M. Z. Liu, H. J. Snaith, M. B. Johnston and L. M. Herz, Homogeneous Emission Line Broadening in the Organo Lead Halide Perovskite CH$_3$NH$_3$PbI$_{3-x}$Cl$_x$, *J. Phys. Chem. Lett.*, 2014, **5**(8), 1300–1306.

8 F. Panzer, S. Baderschneider, T. P. Gujar, T. Unger, S. Bagnich, M. Jakoby, H. Bässler, S. Huettner, J. Köhler, R. Moos, M. Thelakkat, R. Hildner and A. Köhler, Reversible Laser Induced Amplified Spontaneous Emission from Coexisting Tetragonal and Orthorhombic Phases in Hybrid Lead Halide Perovskites, *Adv. Opt. Mater.*, 2016, **4**(6), 917–928.

9 X. X. Wu, M. T. Trinh, D. Niesner, H. M. Zhu, Z. Norman, J. S. Owen, O. Yaffe, B. J. Kudisch and X. Y. Zhu, Trap States in Lead Iodide Perovskites, *J. Am. Chem. Soc.*, 2015, **137**(5), 2089–2096.

10 C. Wehrenfennig, M. Z. Liu, H. J. Snaith, M. B. Johnston and L. M. Herz, Charge Carrier Recombination Channels in the Low-Temperature Phase of Organic-Inorganic Lead Halide Perovskite Thin Films, *APL Mater.*, 2014, **2**(8), 081513.

11 J. Li, A. Dobrovolsky, A. Merdasa, E. L. Unger and I. G. Scheblykin, Luminescent Intermediates and Humidity-Dependent Room-Temperature Conversion of the MAPbI$_3$ Perovskite Precursor, *ACS Omega*, 2018, **3**(10), 14494–14502.

12 Y. Tian, M. Peter, E. Unger, M. Abdellah, K. Zheng, T. Pullerits, A. Yartsev, V. Sundstrom and I. G. Scheblykin,

This journal is © The Royal Society of Chemistry 2020

J. Mater. Chem. C, 2020, **8**, 2289–2300 | **2297**

Mechanistic Insights into Perovskite Photoluminescence Enhancement: Light Curing with Oxygen can Boost Yield Thousandfold, *Phys. Chem. Chem. Phys.*, 2015, **17**(38), 24978–24987.

13 G. Grancini, V. D'Innocenzo, E. R. Dohner, N. Martino, A. R. S. Kandada, E. Mosconi, F. De Angelis, H. I. Karunadasa, E. T. Hoke and A. Petrozza, $CH_3NH_3PbI_3$ Perovskite Single Crystals: Surface Photophysics and their Interaction with the Environment, *Chem. Sci.*, 2015, **6**(12), 7305–7310.

14 D. W. deQuilettes, S. M. Vorpahl, S. D. Stranks, H. Nagaoka, G. E. Eperon, M. E. Ziffer, H. J. Snaith and D. S. Ginger, Impact of Microstructure on Local Carrier Lifetime in Perovskite Solar Cells, *Science*, 2015, **348**(6235), 683–686.

15 Q. Jiang, Y. Zhao, X. Zhang, X. Yang, Y. Chen, Z. Chu, Q. Ye, X. Li, Z. Yin and J. You, Surface Passivation of Perovskite Film for Efficient Solar Cells, *Nat. Photonics*, 2019, **13**(7), 460–466.

16 N. K. Noel, A. Abate, S. D. Stranks, E. S. Parrott, V. M. Burlakov, A. Goriely and H. J. Snaith, Enhanced Photoluminescence and Solar Cell Performance *via* Lewis Base Passivation of Organic Inorganic Lead Halide Perovskites, *ACS Nano*, 2014, **8**(10), 9815–9821.

17 M. Abdi-Jalebi, Z. Andaji-Garmaroudi, S. Cacovich, C. Stavrakas, B. Philippe, J. M. Richter, M. Alsari, E. P. Booker, E. M. Hutter, A. J. Pearson, S. Lilliu, T. J. Savenije, H. Rensmo, G. Divitini, C. Ducati, R. H. Friend and S. D. Stranks, Maximizing and Stabilizing Luminescence from Halide Perovskites with Potassium Passivation, *Nature*, 2018, **555**(7697), 497–501.

18 E. M. Hutter, M. C. Gélvez-Rueda, A. Osherov, V. Bulović, F. C. Grozema, S. D. Stranks and T. J. Savenije, Direct-Indirect Character of the Bandgap in Methylammonium Lead Iodide Perovskite, *Nat. Mater.*, 2017, **16**(1), 115–120.

19 T. Wang, B. Daiber, J. M. Frost, S. A. Mann, E. C. Garnett, A. Walsh and B. Ehrler, Indirect to Direct Bandgap Transition in Methylammonium Lead Halide Perovskite, *Energy Environ. Sci.*, 2017, **10**(2), 509–515.

20 B. Wu, H. F. Yuan, Q. Xu, J. A. Steele, D. Giovanni, P. Puech, J. H. Fu, Y. F. Ng, N. F. Jamaludin, A. Solanki, S. Mhaisalkar, N. Mathews, M. B. J. Roeffaers, M. Grätzel, J. Hofkens and T. C. Sum, Indirect Tail States Formation by Thermal-Induced Polar Fluctuations in Halide Perovskites, *Nat. Commun.*, 2019, **10**, 484.

21 J. H. Fu, N. F. Jamaludin, B. Wu, M. J. Li, A. Solanki, Y. F. Ng, S. Mhaisalkar, C. H. A. Huan and T. C. Sum, Localized Traps Limited Recombination in Lead Bromide Perovskites, *Adv. Energy Mater.*, 2019, **9**(12), 1803119.

22 J. A. Steele, P. Puech, B. Monserrat, B. Wu, R. X. Yang, T. Kirchartz, H. Yuan, G. Fleury, D. Giovanni, E. Fron, M. Keshavarz, E. Debroye, G. Zhou, T. C. Sum, A. Walsh, J. Hofkens and M. B. J. Roeffaers, Role of Electron–Phonon Coupling in the Thermal Evolution of Bulk Rashba-Like Spin-Split Lead Halide Perovskites Exhibiting Dual-Band Photoluminescence, *ACS Energy Lett.*, 2019, 2205–2212.

23 X. Chi, K. Leng, B. Wu, D. Shi, Y. Choy, Z. Chen, Z. Chen, X. Yu, P. Yang, Q.-H. Xu, T. C. Sum, A. Rusydi and K. P. Loh, Elucidating Surface and Bulk Emission in 3D Hybrid Organic-Inorganic Lead Bromide Perovskites, *Adv. Opt. Mater.*, 2018, **6**(15), 1800470.

24 J. Shi, H. Zhang, Y. Li, J. J. Jasieniak, Y. Li, H. Wu, Y. Luo, D. Li and Q. Meng, Identification of High-Temperature Exciton States and their Phase-Dependent Trapping Behaviour in Lead Halide Perovskites, *Energy Environ. Sci.*, 2018, **11**(6), 1460–1469.

25 D. Niesner, O. Schuster, M. Wilhelm, I. Levchuk, A. Osvet, S. Shrestha, M. Batentschuk, C. Brabec and T. Fauster, Temperature-Dependent Optical Spectra of Single-Crystal $(CH_3NH_3) PbBr_3$ Cleaved in Ultrahigh Vacuum, *Phys. Rev. B*, 2017, **95**(7), 075207.

26 B. Murali, S. Dey, A. L. Abdelhady, W. Peng, E. Alarousu, A. R. Kirmani, N. C. Cho, S. P. Sarmah, M. R. Parida, M. I. Saidaminov, A. A. Zhumekenov, J. Y. Sun, M. S. Alias, E. Yengel, B. S. Ooi, A. Amassian, O. M. Bakr and O. F. Mohammed, Surface Restructuring of Hybrid Perovskite Crystals, *ACS Energy Lett.*, 2016, **1**(6), 1119–1126.

27 B. Murali, E. Yengel, C. Yang, W. Peng, E. Alarousu, O. M. Bakr and O. F. Mohammed, The Surface of Hybrid Perovskite Crystals: A Boon or Bane, *ACS Energy Lett.*, 2017, **2**(4), 846–856.

28 S. T. Birkhold, E. Zimmermann, T. Kollek, D. Wurmbrand, S. Polarz and L. Schmidt-Mende, Impact of Crystal Surface on Photoexcited States in Organic-Inorganic Perovskites, *Adv. Funct. Mater.*, 2017, **27**(6), 1604995.

29 F. Chen, C. Zhu, C. X. Xu, P. Fan, F. F. Qin, A. G. Manohari, J. F. Lu, Z. L. Shi, Q. Y. Xu and A. L. Pan, Crystal Structure and Electron Transition Underlying Photoluminescence of Methylammonium Lead Bromide Perovskites, *J. Mater. Chem. C*, 2017, **5**(31), 7739–7745.

30 L. M. Pazos-Outón, M. Szumilo, R. Lamboll, J. M. Richter, M. Crespo-Quesada, M. Abdi-Jalebi, H. J. Beeson, M. Vrucinic, M. Alsari, H. J. Snaith, B. Ehrler, R. H. Friend and F. Deschler, Photon Recycling in Lead Iodide Perovskite Solar Cells, *Science*, 2016, **351**(6280), 1430–1433.

31 Y. Fang, H. Wei, Q. Dong and J. Huang, Quantification of Re-Absorption and Re-Emission Processes to Determine Photon Recycling Efficiency in Perovskite Single Crystals, *Nat. Commun.*, 2017, **8**, 14417.

32 Y. Yamada, T. Yamada, L. Q. Phuong, N. Maruyama, H. Nishimura, A. Wakamiya, Y. Murata and Y. Kanemitsu, Dynamic Optical Properties of $CH_3NH_3PbI_3$ Single Crystals as Revealed by One- and Two-Photon Excited Photoluminescence Measurements, *J. Am. Chem. Soc.*, 2015, **137**(33), 10456–10459.

33 T. Yamada, Y. Yamada, H. Nishimura, Y. Nakaike, A. Wakamiya, Y. Murata and Y. Kanemitsu, Fast Free-Carrier Diffusion in $CH_3NH_3PbBr_3$ Single Crystals Revealed by Time-Resolved One- and Two-Photon Excitation Photoluminescence Spectroscopy, *Adv. Electron. Mater.*, 2016, **2**(3), 1500290.

34 A. Poglitsch and D. Weber, Dynamic Disorder in Methyl-ammoniumtrihalogenoplumbates(II) Observed by Millimeter-Wave Spectroscopy, *J. Chem. Phys.*, 1987, **87**(11), 6373–6378.

35 T. Ishihara, Optical-Properties of PbI-Based Perovskite Structures, *J. Lumin.*, 1994, **60–61**, 269–274.

2298 | *J. Mater. Chem. C*, 2020, **8**, 2289–2300

This journal is © The Royal Society of Chemistry 2020

36 W. G. Kong, Z. Y. Ye, Z. Qi, B. P. Zhang, M. Wang, A. Rahimi-Iman and H. Z. Wu, Characterization of an Abnormal Photoluminescence Behavior upon Crystal-Phase Transition of Perovskite $CH_3NH_3PbI_3$, *Phys. Chem. Chem. Phys.*, 2015, **17**(25), 16405–16411.

37 E. S. Parrott, R. L. Milot, T. Stergiopoulos, H. J. Snaith, M. B. Johnston and L. M. Herz, Effect of Structural Phase Transition on Charge-Carrier Lifetimes and Defects in $CH_3NH_3SnI_3$ Perovskite, *J. Phys. Chem. Lett.*, 2016, **7**(7), 1321–1326.

38 D. Niesner, M. Wilhelm, I. Levchuk, A. Osvet, S. Shrestha, M. Batentschuk, C. Brabec and T. Fauster, Giant Rashba Splitting in $CH_3NH_3PbBr_3$ Organic-Inorganic Perovskite, *Phys. Rev. Lett.*, 2016, **117**(12), 126401.

39 D. Niesner, M. Hauck, S. Shrestha, I. Levchuk, G. J. Matt, A. Osvet, M. Batentschuk, C. Brabec, H. B. Weber and T. Fauster, Structural Fluctuations Cause Spin-Split States in Tetragonal $CH_3NH_3PbI_3$ as Evidenced by the Circular Photogalvanic Effect, *Proc. Natl. Acad. Sci. U. S. A.*, 2018, **115**(38), 9509–9514.

40 S. D. Stranks and P. Plochocka, The Influence of the Rashba Effect, *Nat. Mater.*, 2018, **17**(5), 381–382.

41 L. Leppert, S. E. Reyes-Lillo and J. B. Neaton, Electric Field-and Strain-Induced Rashba Effect in Hybrid Halide Perovskites, *J. Phys. Chem. Lett.*, 2016, **7**(18), 3683–3689.

42 J. M. Richter, K. Chen, A. Sadhanala, J. Butkus, J. P. H. Rivett, R. H. Friend, B. Monserrat, J. M. Hodgkiss and F. Deschler, Direct Bandgap Behavior in Rashba-Type Metal Halide Perovskites, *Adv. Mater.*, 2018, **30**(52), e1803379.

43 F. Zheng, L. Z. Tan, S. Liu and A. M. Rappe, Rashba Spin-Orbit Coupling Enhanced Carrier Lifetime in $CH_3NH_3PbI_3$, *Nano Lett.*, 2015, **15**(12), 7794–7800.

44 T. Etienne, E. Mosconi and F. De Angelis, Dynamical Origin of the Rashba Effect in Organohalide Lead Perovskites: A Key to Suppressed Carrier Recombination in Perovskite Solar Cells?, *J. Phys. Chem. Lett.*, 2016, **7**(9), 1638–1645.

45 M. Kepenekian and J. Even, Rashba and Dresselhaus Couplings in Halide Perovskites: Accomplishments and Opportunities for Spintronics and Spin-Orbitronics, *J. Phys. Chem. Lett.*, 2017, **8**(14), 3362–3370.

46 T. Kirchartz and U. Rau, Decreasing Radiative Recombination Coefficients *via* an Indirect Band Gap in Lead Halide Perovskites, *J. Phys. Chem. Lett.*, 2017, **8**(6), 1265–1271.

47 D. A. Egger, A. Bera, D. Cahen, G. Hodes, T. Kirchartz, L. Kronik, R. Lovrincic, A. M. Rappe, D. R. Reichman and O. Yaffe, What Remains Unexplained about the Properties of Halide Perovskites?, *Adv. Mater.*, 2018, **30**(20), e1800691.

48 K. Frohna, T. Deshpande, J. Harter, W. Peng, B. A. Barker, J. B. Neaton, S. G. Louie, O. M. Bakr, D. Hsieh and M. Bernardi, Inversion Symmetry and Bulk Rashba Effect in Methylammonium Lead Iodide Perovskite Single Crystals, *Nat. Commun.*, 2018, **9**, 1829.

49 C. L. Davies, M. R. Filip, J. B. Patel, T. W. Crothers, C. Verdi, A. D. Wright, R. L. Milot, F. Giustino, M. B. Johnston and L. M. Herz, Bimolecular Recombination in Methylammonium Lead Triiodide Perovskite is an Inverse Absorption Process, *Nat. Commun.*, 2018, **9**(1), 293.

50 P. Azarhoosh, S. McKechnie, J. M. Frost, A. Walsh and M. van Schilfgaarde, Research Update: Relativistic Origin of Slow Electron-Hole Recombination in Hybrid Halide Perovskite Solar Cells, *APL Mater.*, 2016, **4**(9), 091501.

51 W. Du, S. A. Ghetmiri, B. R. Conley, A. Mosleh, A. Nazzal, R. A. Soref, G. Sun, J. Tolle, J. Margetis, H. A. Naseem and S.-Q. Yu, Competition of Optical Transitions Between Direct and Indirect Bandgaps in $Ge_{1-x}Sn_x$, *Appl. Phys. Lett.*, 2014, **105**(5), 051104.

52 S. Al-Kabi, S. Ghetmiri, J. Margetis, W. Du, A. Mosleh, M. Alher, W. Dou, J. Grant, G. Sun, R. Soref, J. Tolle, B. Li, M. Mortazavi, H. Naseem and S. Q. Yu, Optical Characterization of Si-Based $Ge_{1-x}Sn_x$ Alloys with Sn Compositions up to 12%, *J. Electron. Mater.*, 2016, **45**(4), 2133–2141.

53 D. Stange, S. Wirths, N. von den Driesch, G. Mussler, T. Stoica, Z. Ikonic, J. M. Hartmann, S. Mantl, D. Grützmacher and D. Buca, Optical Transitions in Direct-Bandgap $Ge_{1-x}Sn_x$ Alloys, *ACS Photonics*, 2015, **2**(11), 1539–1545.

54 S. Wirths, R. Geiger, N. von den Driesch, G. Mussler, T. Stoica, S. Mantl, Z. Ikonic, M. Luysberg, S. Chiussi, J. M. Hartmann, H. Sigg, J. Faist, D. Buca and D. Grutzmacher, Lasing in Direct-Bandgap GeSn Alloy Grown on Si, *Nat. Photonics*, 2015, **9**(2), 88–92.

55 T. W. Jones, A. Osherov, M. Alsari, M. Sponseller, B. C. Duck, Y. K. Jung, C. Settens, F. Niroui, R. Brenes, C. V. Stan, Y. Li, M. Abdi-Jalebi, N. Tamura, J. E. Macdonald, M. Burghammer, R. H. Friend, V. Bulovic, A. Walsh, G. J. Wilson, S. Lilliu and S. D. Stranks, Lattice Strain Causes Non-Radiative Losses in Halide Perovskites, *Energy Environ. Sci.*, 2019, **12**(2), 596–606.

56 X. Y. Li, Y. Q. Luo, M. V. Holt, Z. H. Cai and D. P. Fenning, Residual Nanoscale Strain in Cesium Lead Bromide Perovskite Reduces Stability and Shifts Local Luminescence, *Chem. Mater.*, 2019, **31**(8), 2778–2785.

57 Goodfellow GmbH, Datasheet polyethylene terephthalate (Polyester, PET, PETP); available from goodfellow.com/E/Polyethylene-terephthalate.html, last accessed September 3, 2019.

58 Polymerdatabase, Datasheet poly(ethylene terephthalate) (PET), available from polymerdatabase.com/Commercial%20Polymers/PET.html, last accessed September 3, 2019.

59 H. A. Schaeffer and R. Langfeld, *Werkstoff Glas*, Springer Vieweg, Berlin, Heidelberg, Germany, 2014, p. 46.

60 S. Singh, C. Li, F. Panzer, K. L. Narasimhan, A. Graeser, T. P. Gujar, A. Köhler, M. Thelakkat, S. Huettner and D. Kabra, Effect of Thermal and Structural Disorder on the Electronic Structure of Hybrid Perovskite Semiconductor $CH_3NH_3PbI_3$, *J. Phys. Chem. Lett.*, 2016, **7**(15), 3014–3021.

61 T. J. Jacobsson, L. J. Schwan, M. Ottosson, A. Hagfeldt and T. Edvinsson, Determination of Thermal Expansion Coefficients and Locating the Temperature-Induced Phase Transition in Methylammonium Lead Perovskites Using X-ray Diffraction, *Inorg. Chem.*, 2015, **54**(22), 10678–10685.

62 J. Zhao, Y. Deng, H. Wei, X. Zheng, Z. Yu, Y. Shao, J. E. Shield and J. Huang, Strained Hybrid Perovskite Thin Films and Their Impact on the Intrinsic Stability of Perovskite Solar Cells, *Sci. Adv.*, 2017, **3**(11), eaao5616.

This journal is © The Royal Society of Chemistry 2020

J. Mater. Chem. C, 2020, **8**, 2289–2300 | **2299**

63 A. Osherov, E. M. Hutter, K. Galkowski, R. Brenes, D. K. Maude, R. J. Nicholas, P. Plochocka, V. Bulovic, T. J. Savenije and S. D. Stranks, The Impact of Phase Retention on the Structural and Optoelectronic Properties of Metal Halide Perovskites, *Adv. Mater.*, 2016, **28**(48), 10757–10763.

64 F. Panzer, H. Bässler and A. Köhler, Temperature Induced Order-Disorder Transition in Solutions of Conjugated Polymers Probed by Optical Spectroscopy, *J. Phys. Chem. Lett.*, 2017, **8**(1), 114–125.

65 X. P. Zheng, B. Chen, J. Dai, Y. J. Fang, Y. Bai, Y. Z. Lin, H. T. Wei, X. C. Zeng and J. S. Huang, Defect Passivation in Hybrid Perovskite Solar Cells Using Quaternary Ammonium Halide Anions and Cations, *Nat. Energy*, 2017, **2**(7), 17102.

66 S. P. Sarmah, V. M. Burlakov, E. Yengel, B. Murali, E. Alarousu, A. M. El-Zohry, C. Yang, M. S. Alias, A. A. Zhumekenov, M. I. Saidaminov, N. Cho, N. Wehbe, S. Mitra, I. Ajia, S. Dey, A. E. Mansour, M. Abdelsamie, A. Amassian, I. S. Roqan, B. S. Ooi, A. Goriely, O. M. Bakr and O. F. Mohammed, Double Charged Surface Layers in Lead Halide Perovskite Crystals, *Nano Lett.*, 2017, **17**(3), 2021–2027.

67 R. W. Boyd, *Nonlinear Optics*, Academic Press, Burlington, USA, 3rd edn, 2008, pp. 549–559.

68 M. Göppert-Mayer, Über Elementarakte mit zwei Quantensprüngen, *Ann. Phys.*, 1931, **401**(3), 273–294.

69 G. Nagamine, J. O. Rocha, L. G. Bonato, A. F. Nogueira, Z. Zaharieva, A. A. R. Watt, C. H. de Brito Cruz and L. A. Padilha, Two-Photon Absorption and Two-Photon-Induced Gain in Perovskite Quantum Dots, *J. Phys. Chem. Lett.*, 2018, **9**(12), 3478–3484.

70 T. W. Crothers, R. L. Milot, J. B. Patel, E. S. Parrott, J. Schlipf, P. Müller-Buschbaum, M. B. Johnston and L. M. Herz, Photon Reabsorption Masks Intrinsic Bimolecular Charge-Carrier Recombination in $CH_3NH_3PbI_3$ Perovskite, *Nano Lett.*, 2017, **17**(9), 5782–5789.

71 S. De Wolf, J. Holovsky, S. J. Moon, P. Loper, B. Niesen, M. Ledinsky, F. J. Haug, J. H. Yum and C. Ballif, Organometallic Halide Perovskites: Sharp Optical Absorption Edge and Its Relation to Photovoltaic Performance, *J. Phys. Chem. Lett.*, 2014, **5**(6), 1035–1039.

72 A. Sadhanala, F. Deschler, T. H. Thomas, S. E. Dutton, K. C. Goedel, F. C. Hanusch, M. L. Lai, U. Steiner, T. Bein, P. Docampo, D. Cahen and R. H. Friend, Preparation of Single-Phase Films of $CH_3NH_3Pb(I_{1-x}Br_{-x})_3$ with Sharp Optical Band Edges, *J. Phys. Chem. Lett.*, 2014, **5**(15), 2501–2505.

73 V. D'Innocenzo, G. Grancini, M. J. Alcocer, A. R. Kandada, S. D. Stranks, M. M. Lee, G. Lanzani, H. J. Snaith and A. Petrozza, Excitons *Versus* Free Charges in Organo-Lead Tri-Halide Perovskites, *Nat. Commun.*, 2014, **5**, 3586.

74 M. Ledinsky, T. Schönfeldová, J. Holovský, E. Aydin, Z. Hájková, L. Landová, N. Neyková, A. Fejfar and S. De Wolf, Temperature Dependence of the Urbach Energy in Lead Iodide Perovskites, *J. Phys. Chem. Lett.*, 2019, **10**(6), 1368–1373.

75 L. J. Phillips, A. M. Rashed, R. E. Treharne, J. Kay, P. Yates, I. Z. Mitrovic, A. Weerakkody, S. Hall and K. Durose, Dispersion Relation Data for Methylammonium Lead Triiodide Perovskite Deposited on a (100) Silicon Wafer Using a Two-Step Vapour-Phase Reaction Process, *Data Brief*, 2015, **5**, 926–928.

76 R. Brenes, M. Laitz, J. Jean, D. W. de Quilettes and V. Bulovic, Benefit from Photon Recycling at the Maximum-Power Point of State-of-the-Art Perovskite Solar Cells, *Phys. Rev. Appl.*, 2019, **12**(1), 014017.

77 I. Dursun, Y. Z. Zheng, T. L. Guo, M. De Bastiani, B. Turedi, L. Sinatra, M. A. Hague, B. Sun, A. A. Zhumekenov, M. I. Saidaminov, F. P. G. de Arquer, E. H. Sargent, T. Wu, Y. N. Gartstein, O. M. Bakr, O. F. Mohammed and A. V. Malko, Efficient Photon Recycling and Radiation Trapping in Cesium Lead Halide Perovskite Waveguides, *ACS Energy Lett.*, 2018, **3**(7), 1492–1498.

78 J. Rheims, J. Koser and T. Wriedt, Refractive-Index Measurements in the Near-IR Using an Abbe Refractometer, *Meas. Sci. Technol.*, 1997, **8**(6), 601–605.

79 L. Q. Phuong, Y. Nakaike, A. Wakamiya and Y. Kanemitsu, Free Excitons and Exciton-Phonon Coupling in $CH_3NH_3PbI_3$ Single Crystals Revealed by Photocurrent and Photoluminescence Measurements at Low Temperatures, *J. Phys. Chem. Lett.*, 2016, **7**(23), 4905–4910.

80 K. Kojima, K. Ikemura, K. Matsumori, Y. Yamada, Y. Kanemitsu and S. F. Chichibu, Internal Quantum Efficiency of Radiation in a Bulk $CH_3NH_3PbBr_3$ Perovskite Crystal Quantified by Using the Omnidirectional Photoluminescence Spectroscopy, *APL Mater.*, 2019, **7**(7), 071116.

81 M. I. Saidaminov, A. L. Abdelhady, B. Murali, E. Alarousu, V. M. Burlakov, W. Peng, I. Dursun, L. F. Wang, Y. He, G. Maculan, A. Goriely, T. Wu, O. F. Mohammed and O. M. Bakr, High-Quality Bulk Hybrid Perovskite Single Crystals Within Minutes by Inverse Temperature Crystallization, *Nat. Commun.*, 2015, **6**, 7586.

82 W. Peng, X. H. Miao, V. Adinolfi, E. Alarousu, O. El Tall, A. H. Emwas, C. Zhao, G. Walters, J. K. Liu, O. Ouellette, J. Pan, B. Murali, E. H. Sargent, O. F. Mohammed and O. M. Bakr, Engineering of $CH_3NH_3PbI_3$ Perovskite Crystals by Alloying Large Organic Cations for Enhanced Thermal Stability and Transport Properties, *Angew. Chem., Int. Ed.*, 2016, **55**(36), 10686–10690.

83 D. Shi, V. Adinolfi, R. Comin, M. J. Yuan, E. Alarousu, A. Buin, Y. Chen, S. Hoogland, A. Rothenberger, K. Katsiev, Y. Losovyj, X. Zhang, P. A. Dowben, O. F. Mohammed, E. H. Sargent and O. M. Bakr, Low Trap-State Density and Long Carrier Diffusion in Organolead Trihalide Perovskite Single Crystals, *Science*, 2015, **347**(6221), 519–522.

84 T. P. Gujar and M. Thelakkat, Highly Reproducible and Efficient Perovskite Solar Cells with Extraordinary Stability from Robust $CH_3NH_3PbI_3$: Towards Large-Area Devices, *Energy Technol.*, 2016, **4**(3), 449–457.

85 F. Panzer, S. Baderschneider, T. P. Gujar, T. Unger, S. Bagnich, M. Jakoby, H. Bässler, S. Huettner, J. Köhler, R. Moos, M. Thelakkat, R. Hildner and A. Köhler, Reversible Laser-Induced Amplified Spontaneous Emission from Coexisting Tetragonal and Orthorhombic Phases in Hybrid Lead Halide Perovskites, *Adv. Opt. Mater.*, 2016, **4**(6), 917–928.

2300 | *J. Mater. Chem. C*, 2020, **8**, 2289–2300

This journal is © The Royal Society of Chemistry 2020